Ab Initio MO Study of the Full Cycle of Olefin Hydroformylation Catalyzed by a Rhodium Complex, RhH(CO)$_2$(PH$_3$)$_2$

Toshiaki Matsubara,[†] Nobuaki Koga,[‡,§] Yanbo Ding,[‡]
Djamaladdin G. Musaev,[†] and Keiji Morokuma*,[†,‡]

*Cherry L. Emerson Center for Scientific Computation and Department of Chemistry,
Emory University, Atlanta, Georgia 30322, Institute for Molecular Science, Myodaiji,
Okazaki 444, Japan, and School of Informatics and Sciences and Graduate School of
Human Informatics, Nagoya University, Nagoya 464-01, Japan*

The potential energy profile for the full cycle of olefin hydroformylation catalyzed by RhH-(CO)$_2$(PH$_3$)$_2$, consisting of olefin coordination and insertion, CO insertion, H$_2$ oxidative addition, and aldehyde reductive elimination, as well as ligand coordination and dissociation, is investigated using the ab initio molecular orbital method. Structures of nearly all isomers of intermediates and transition states involved in each step are determined mainly at the Hartree−Fock level, and the potential energy profile is calculated at MP2 and MP4 levels. The site preference for trigonal-bipyramidal intermediates and transition states discriminates possible paths of the catalysis. The coordinatively unsaturated intermediates are strongly coordinated and stabilized by a solvent olefin molecule, while the transition states are not solvated. The energetic and entropic effects of solvation play the critical role in determining the activation free energies. Including the solvent effect, the H$_2$ oxidative addition step from a solvated intermediate has one of the highest barriers, consisting of desolvation energy and the intrinsic activation energy.

Introduction

The development of computational techniques such as the ab initio molecular orbital (MO) theory has made it possible to carry out calculations for organometallic compounds. Many theoretical studies have been published on elementary reactions of organometallic compounds,[1] including olefin insertion,[2] CO insertion,[2e,3] oxidative addition,[4−9] and reductive elimination,[5,9] all of which are important reaction steps of many catalytic cycles. Studies of full catalytic cycles involving series of many elementary reactions, however, still remain as one of the theoretical challenges. Although our group some time ago reported the first ab initio MO study of the full cycle for homogeneous olefin hydrogenation[10] catalyzed by a Rh(I) catalyst, aside from our recent study on the full cycle of olefin hydroboration catalyzed by a Rh(I) catalyst,[11] there are still only a few examples.[12] We believe that these theoretical studies shed new light for better understanding of the basics of catalysis and for the design and exploration of new reactions catalyzed by organometallic compounds. In the present paper, we have investigated with the ab initio method the full cycle of the hydroformylation reaction CH$_2$CH$_2$ + H$_2$ + CO → CH$_3$CH$_2$CHO catalyzed by a Rh(I) complex.

Hydroformylation of olefin,[13] as well as hydrogenation of olefin,[14] is widely known as a typical homogeneous reaction catalyzed by a Rh(I) complex. Although ex-

[†] Emory University.
[‡] Institute for Molecular Science.
[§] Nagoya University.
[⊗] Abstract published in *Advance ACS Abstracts,* February 15, 1997.
(1) (a) Dedieu, A. In *Topics in Physical Organometallic Chemistry*; Gielen, M. F., Ed.; Freund Publishing House: London, 1985; Vol. 1, p 1. (b) Koga, N.; Morokuma, K. In *Topics in Physical Organometallic Chemistry*; Gielen, M. F., Ed.; Freund Publishing House: London, 1989; Vol. 3, p 1.
(2) (a) Dedieu, A. *Inorg. Chem.* **1981,** *20,* 2803. (b) Jolly, C. A.; Marynick, D. S. *J. Am. Chem. Soc.* **1989,** *111,* 7968. (c) Kawamura-Kuribayashi, H.; Koga, N.; Morokuma, K. *J. Am. Chem. Soc.* **1992,** *114,* 2359. (d) Siegbahn, P. E. M. *J. Am. Chem. Soc.* **1993,** *115,* 5803. (e) Koga, N.; Morokuma, K. *NATO ASI Ser., Ser. C* **1986,** *176,* 351. (f) Koga, N.; Obara, S.; Kitaura, K.; Morokuma, K. *J. Am. Chem. Soc.* **1985,** *107,* 7109.
(3) (a) Sakaki, S.; Kitaura, K.; Morokuma, K.; Ohkubo, K. *J. Am. Chem. Soc.* **1983,** *105,* 2280. (b) Koga, N.; Morokuma, K. *J. Am. Chem. Soc.* **1985,** *107,* 7230. (c) Koga, N.; Morokuma, K. *J. Am. Chem. Soc.* **1986,** *108,* 6136. (d) Koga, N.; Morokuma, K. *New. J. Chem.* **1991,** *15,* 749.
(4) (a) Kitaura, K.; Obara, S.; Morokuma, K. *J. Am. Chem. Soc.* **1981,** *103,* 2891. (b) Noell, J. O.; Hay, P. J. *J. Am. Chem. Soc.* **1982,** *104,* 4578.
(5) (a) Obara, S.; Kitaura, K.; Morokuma, K. *J. Am. Chem. Soc.* **1984,** *106,* 7482. (b) Low, J. J.; Goddard, W. A., III. *J. Am. Chem. Soc.* **1984,** *106,* 6928. (c) Low, J. J.; Goddard, W. A., III. *J. Am. Chem. Soc.* **1986,** *108,* 6115. (d) Low, J. J.; Goddard, W. A., III. *Organometallics* **1986,** *5,* 609.
(6) Hay, P. J. *J. Am. Chem. Soc.* **1987,** *109,* 705.
(7) (a) Sargent, A. L.; Hall, M. B. *Inorg. Chem.* **1992,** *31,* 317. (b) Sargent, A. L.; Hall, M. B.; Guest, M. F. *J. Am. Chem. Soc.* **1992,** *114,* 517.

(8) (a) Koga, N.; Morokuma, K. *J. Phys. Chem.* **1990,** *94,* 5454. (b) Sakaki, S.; Ikei, M. *J. Am. Chem. Soc.* **1991,** *113,* 5063. (c) Sakaki, S.; Ikei, M. *J. Am. Chem. Soc.* **1993,** *115,* 2373. (d) Koga, N.; Morokuma, K. *J. Am. Chem. Soc.* **1993,** *115,* 6883.
(9) Low, J. J.; Goddard, W. A., III. *J. Am. Chem. Soc.* **1984,** *106,* 8231.
(10) (a) Koga, N.; Daniel, C.; Han, J.; Fu, X. Y.; Morokuma, K. *J. Am. Chem. Soc.* **1987,** *109,* 3455. (b) Daniel, C.; Koga, N.; Han, J.; Fu, X. Y.; Morokuma, K. *J. Am. Chem. Soc.* **1988,** *110,* 3773.
(11) Musaev, D. G.; Mebel, A. M.; Morokuma, K. *J. Am. Chem. Soc.* **1994,** *116,* 10693.
(12) For example: Dedieu A. *Inorg. Chem..* **1980,** *19,* 375.
(13) (a) Evans, D.; Osborn, J. A.; Wilkinson, G. *J. Chem. Soc. A* **1968,** 3133. (b) Evans, D.; Yagupsky, G.; Wilkinson, G. *J. Chem. Soc. A* **1968,** 2660. (c) Brown, C. K.; Wilkinson, G. *J. Chem. Soc. A* **1970,** 2753.
(14) (a) Parshall, G. W. *Homogeneous Catalysis. The Application and Chemistry of Catalysis by Soluble Transition Metal Complexes*; John Wiley & Sons: New York, 1980. (b) Botteghi, C.; Glandiali, S.; Bellagamba; Ercoli, R.; Gambna, A. *Chim. Ind. (Milan)* **1980,** *62,* 604. (c) Pino, P. *J. Organomet. Chem.* **1980,** *200,* 223.

Scheme 1. Mechanism of Hydroformylation Catalyzed by RhH(CO)₂(PPh₃)₂ Proposed by Wilkinson et al.
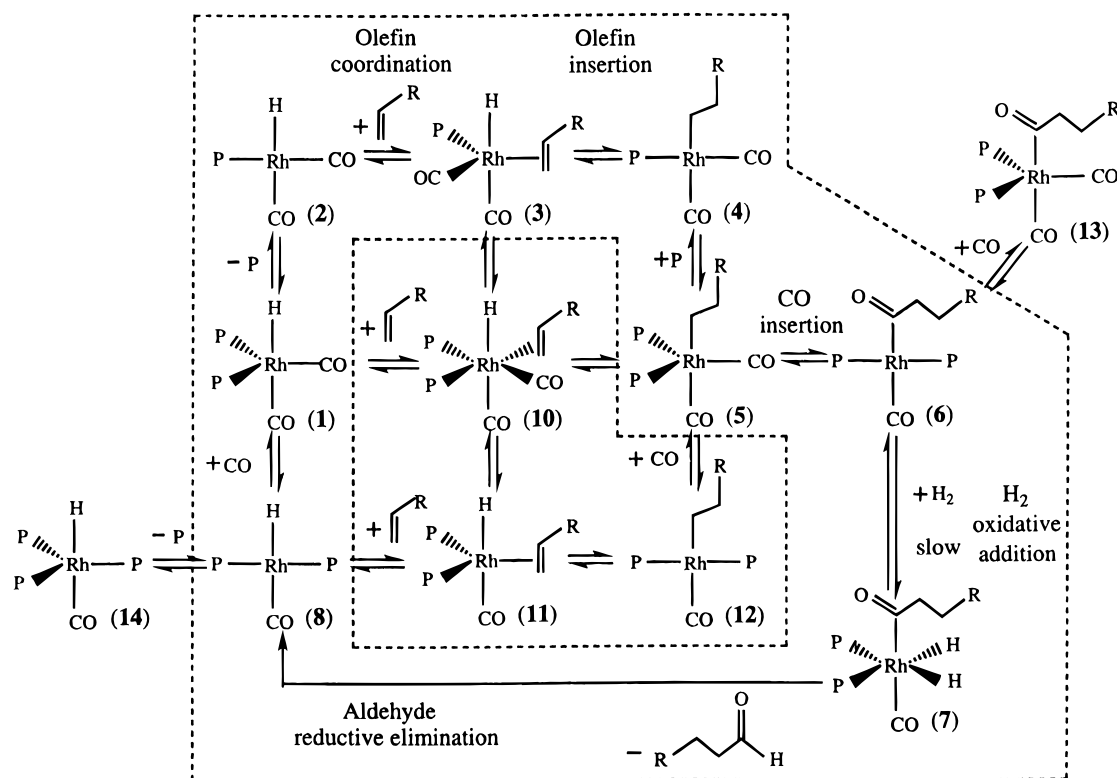
tensive experimental studies on olefin hydroformylation have been made because of its importance in industry[15,16] and a conceivable mechanism has been proposed by 1970 by Wilkinson et al.,[13] the mechanism of the catalytic cycle is still poorly established.[17] The proposed mechanism of the catalytic cycle mediated by RhH(CO)₂-(PPh₃)₂, **1**, can be represented as in Scheme 1. The precursor RhH(CO)(PPh₃)₃, **14**, is readily converted, under CO atmosphere through PPh₃–CO ligand exchange, into complex **1**, which enters into the catalytic cycle. In the first step of the cycle, an olefin coordinates to the Rh atom, so that olefin insertion can take place. Wilkinson et al. have proposed the associative mechanism **1** → **10** rather than the dissociative mechanism **1** → **2** → **3** or **1** → **8** → **11**. However, one should note that the associative mechanism which includes the 20-electron six-coordinate complex **10** is unfavorable both electronically and sterically. On the other hand, two intermediates are possible in the dissociative mechanism:[13bc,18] RhH(CO)₂(PPh₃), **2**, and RhH(CO)(PPh₃)₂, **8**, which are derived from **1** by PPh₃ and CO dissociation, respectively. The industrially important linear-chain aldehyde is produced selectively under high PPh₃ concentration and low CO pressure conditions.[13a,17a,19] However, olefin coordination to **8** is apparently less favorable kinetically than that to **2** because the two phosphine ligands mutually *trans* in **8** would sterically inhibit an olefin from attacking **8**. Brown et al. have

suggested for the 5-phenyl-5*H*-dibenzophosphole analogs by means of NMR spectroscopy that olefin coordinates the intermediate **2** selectively.[20] Therefore, we restricted our analysis to the phosphine ligand dissociation mechanism **1** → **2** → **3**. The olefin coordination is followed by olefin insertion, **3** → **4**, PPh₃ coordination, **4** → **5**, CO insertion, **5** → **6**, H₂ oxidative addition, **6** → **7**, and aldehyde reductive elimination, **7** → **8**, as surrounded by the dotted lines in Scheme 1.

Although direct isolation or observation of labile intermediates involved in the catalytic cycle is difficult, some related derivatives and analogs have been detected in situ using model reactions, demonstrating that some parts of the catalytic cycle actually take place.[20b,21] The intermediate Rh(COEt)(CO)₂(PPh₃)₂, **13**, has been obtained in the stoichiometric reaction of **1** with C₂H₄.[18] The complex **13**, stable in solution only in the presence of excess CO, reacts with H₂, losing CO, to give aldehyde.[18a] The iridium analog of **1**, IrH(CO)₂(PPh₃)₂, also reacts with C₂H₄ to give unstable Ir(COEt)(CO)-(PPh₃)₂ at −70 °C.[18a] The reaction of IrH(CO)₂(PPh₃)₂ with C₂H₄ and CO gives a stable intermediate, Ir-(COEt)(CO)₂(PPh₃)₂, which reacts with H₂ much more slowly than its Rh analog to give aldehyde and IrH-(CO)₂(PPh₃)₂.[18a] The complex Ir(Et)(CO)₂(dppe) undergoes CO insertion to form Ir(COEt)(CO)₂(dppe), which reacts slowly with H₂ to produce IrH₂(COEt)(CO)(dppe), and finally reductive elimination of aldehyde occurs with concomitant formation of IrH₃(CO)(dppe), demonstrating that elementary reaction steps of CO insertion, H₂ oxidative addition, and aldehyde reductive elimination take place.[22] The rate-determining step is generally

(15) Tolman, C. A.; Faller, J. W. In *Homogeneous Catalysis with Metal Phosphine Complexes*; Plgnolet L. H., Ed.; Plenum Press: New York, 1983.

(16) Pruett, R. L. *Adv. Organomet. Chem.* **1979**, *17*, 1.

(17) (a) Hjortkjaer, J. *J. Mol. Catal.* **1979**, *5*, 377. (b) Chan, A. S. C.; Carroll, W. E.; Willis, D. E. *J. Mol. Catal.* **1983**, *19*, 377. (c) Hjortkjaer, J.; Toromanova-Petrova, P. *J. Mol. Catal.* **1989**, *50*, 203.

(18) (a) Yagupsky, G.; Brown, C. K.; Wilkinson, G. *J. Chem. Soc., Chem. Commun.* **1969**, 1244. (b) Yagupsky, G.; Brown, C. K.; Wilkinson, G. *J. Chem. Soc. A* **1970**, 1392.

(19) Pruett, R. L.; Smith, J. A. *J. Org. Chem.* **1969**, *34*, 327.

(20) (a) Brown, J. M.; Channing, L. R.; Kent, A. G.; Sidebottomm, P. J. *J. Chem. Soc., Chem. Commun.* **1982**, 721. (b) Brown, J. M.; Kent, A. G. *J. Chem. Soc., Perkin Trans. 2* **1987**, 1597.

(21) Brown, J. M.; Kent, A. G. *J. Chem. Soc., Chem. Commun.* **1982**, 723.

believed to be the H_2 oxidative addition step on the basis of the pressure dependence of the overall reaction rate.[13a,b]

We have already reported an ab initio theoretical study for one of the above steps, olefin insertion for a model olefin, C_2H_4, and a model phosphine, PH_3.[23] The intermediate $RhH(C_2H_4)(CO)_2(PH_3)$, corresponding to **3**, has a trigonal-bipyramidal structure (TBP), and its site preference for axial hydride and equatorial ethylene has been demonstrated. While in the d^8 TBP structure the axial d orbital, e.g. d_{z^2}, is formally vacant and thus a strong σ bond is formed with axial hydride, the d orbitals in the equatorial plane, e.g. $d_{x^2-y^2}$ and d_{xy}, are occupied and therefore appropriate for back-donation, favoring equatorial ethylene coordination. The intramolecular rearrangement between TBP equilibrium structures has been found to take place with a small intrinsic barrier, passing through square-pyramidal (SPy) transition states (TSs) via the Berry pseudorotation (BPR). The intramolecular olefin insertion proceeds through an SPy transition state with basal olefin and basal hydride.

Our goals of the present paper are (i) to determine the geometrical structures of all transition states as well as intermediates involved in the proposed mechanism of the catalytic cycle, (ii) to determine the potential energy profile of the entire catalytic process, (iii) to assess the role of solvation, and (iv) to identify the rate-determining step.[24] Although the solvation to the coordinatively unsaturated species in organometallic reactions in solution has long been suggested experimentally, the importance of solvent effects has not been dealt with in theoretical studies. We believe that this is the first paper to demonstrate that the coordination of hydrocarbon solvent molecules to coordinatively unsaturated intermediates is one of the most crucial factors in determining the potential energy profile of an entire catalytic cycle.

In the calculation, as in the previous study,[23] we used ethylene as the model olefin. As for phosphine ligand, although the PPh_3 was used in experiments, we were forced to use PH_3 due to the computational limitations. We will, however, discuss the effect of bulky phosphine qualitatively as we examine various intermediates and transition states. Since the solvent used experimentally was benzene or an alkene, we used ethylene as its model. In the rest of the paper, to identify the intermediates, we will use the same compound numbers as those in Scheme 1, although PPh_3 is replaced by PH_3 and ethylene is used.[25]

Method of Computation

We used the GAUSSIAN series of program[26] for all the calculations. All geometries of transition states as well as intermediates were optimized at the restricted Hartree−Fock (RHF) level under the effective core potential (ECP) approximation. For the energetics, the electron correlation calculations were performed with the frozen-core second-order Møller−Plesset (MP2) perturbation method for the RHF optimized structures. We used two basis sets, basis set I for the HF geometrical optimization and basis set II for the MP2 energy calculation and higher level calculations. Basis set I consists of the split-valence 3-21G basis functions for carbon, oxygen, and hydrogen of CO, C_2H_4, and hydride ligands and the STO-2G minimal basis functions for spectator PH_3 ligands. For Rh, we used the valence double-ζ basis functions (3s,3p, 4d)/[2s,2p,2d] in conjunction with the Hay−Wadt relativistic ECP to replace core electrons up to 4p.[27] Basis set II consists of (11s,8p)/[4s,3p] for phosphine, (8s,5p)/[3s,2p] for carbon and oxygen and (5s)/[3s] for hydrogen of CO, C_2H_4, and the hydride ligand, (4s)/[2s] for hydrogen of PH_3, and a split-valence set with triple-ζ 4d, (5s,6p,4d)/[3s,3p,3d], for Rh, with the Hay−Wadt relativistic ECP to replace core electrons up to 3d.[28] We used the small basis set I for geometry optimization at the RHF level to retain the consistency with our previous calculations of the olefin insertion step.[23] In order to ascertain the reliability of the RHF optimized geometries, we also performed MP2 geometry optimization with basis set II for the first ligand dissociation and ethylene coordination steps: $\mathbf{1} \rightarrow \mathbf{2} \rightarrow \mathbf{3}$. Furthermore, MP4SDQ/II single-point calculations were performed for some key reaction steps at the RHF optimized geometry to obtain the final energetics.

In the geometry optimization, the rotation of PH_3 groups around the metal−phosphine axes was frozen in order to save computational time, as the energy change by this rotation was very small. (For instance, the energy change even in **8b** with two mutually *cis* phosphine ligands was less than 1 kcal/mol.) Otherwise, all the geometrical parameters were fully optimized, except that symmetries were assumed for some structures. We will use the standard notation to describe the computational method, such as MP2/II//RHF/I, which means an MP2 energy calculation with basis set II at the structure determined at the RHF level with basis set I. The thermochemical parameters were calculated at the RHF/I level with a scale factor of 0.89 for calculated vibrational frequencies.

Intermediates Involved in the Catalytic Cycle

In the catalytic cycle proposed by Wilkinson et al., several four-, five-, and six-coordinate intermediates are involved. From the five-coordinate parent complex **1**, four- and five-coordinate intermediates are generated in turn. A six-coordinate intermediate, **7**, is generated by H_2 oxidative addition to the four-coordinate intermediate **6**, where the oxidation number of rhodium is changed from I to III, and it is reduced again to a four-coordinate intermediate, **8**, by reductive elimination of aldehyde. As shown previously by us,[23] the BPR rearrangement among the isomers of the intermediate **3** can take place with a very small intrinsic barrier. Similar rearrangements may take place among isomers of the other five-coordinate intermediates **1** and **5**. Four- and six-coordinate intermediates connecting them in the catalytic cycle necessarily also have various isomers. For instance, the two isomers of the intermediate **3** are connected to the *cis* and *trans* isomer of the intermediate **4**, respectively.[23]

(22) Duetsch, P. P.; Eisenberg, R. *Organometallics* **1990**, *9*, 709.

(23) Koga, N.; Jin, S. Q.; Morokuma, K. *J. Am. Chem. Soc.* **1988**, *110*, 3417.

(24) For preliminary reports of the present work, see: (a) Ding, Y.; Koga, N.; Morokuma, K. *Abstracts of Papers*, 37th Symposium on Organometallic Chemistry, Osaka, Japan, Oct 1990; Kinki Chemical Society: Osaka, Japan, 1990; pp 61−63. (b) Matsubara, T.; Musaev, D. G.; Ding, Y.; Koga, N.; Morokuma, K. *Abstracts of Papers*, 41st Symposium on Organometallic Chemistry, Osaka, Japan, Oct 1994; Kinki Chemical Society: Osaka, Japan, 1994; pp 196−198.
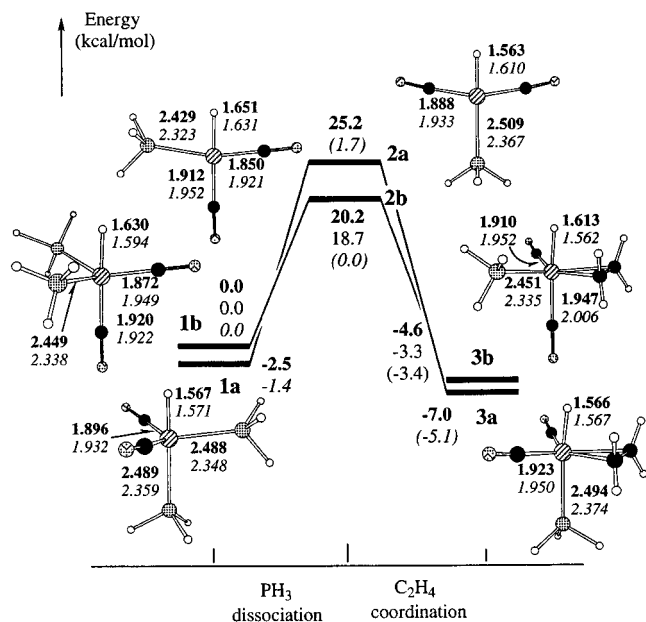
(25) For a computational method and calculation where molecular orbital and molecular mechanics methods are combined to treat bulky substituents, see: (a) Maseras, F.; Morokuma, K. *J. Comput. Chem.* **1995**, *16*, 1170. (b) Matsubara, T.; Maseras, F.; Koga, N.; Morokuma, K. *J. Phys. Chem.* **1996**, *100*, 2573.

(26) Frisch, M. J.; Trucks, G. W.; Head-Gordon, M; Gill, P. M. W.; Wong, M. W.; Foresman, J. B.; Johnson, B. G.; Schlegel, H. B.; Robb, M. A.; Replogle, E. S.; Gomperts, R.; Andres, J. L.; Raghavachari, K.; Binkley, J. S.; Gonzales, C.; Martin, R. L.; Fox, D. J.; DeFrees, D. J.; Baker, J.; Stewart, J. J. A.; Pople, J. A. *GAUSSIAN-92*; Gaussian Inc.: Pittsburgh, PA, 1992.

(27) Hay, P. J.; Wadt, W. R. *J. Chem. Phys.* **1985**, *82*, 270.

(28) Hay, P. J.; Wadt, W. R. *J. Chem. Phys.* **1985**, *82*, 299.

Figure 1. MP2/II (in bold) and RHF/I optimized structures (Å, deg) of the isomers of intermediates **1−3**, and their energies (kcal/mol) at MP2/II//MP2/II (in bold), MP2/II//RHF/I, and RHF/I//RHF/I (in italic) levels, relative to **1b**, except for the RHF numbers in parentheses, which are relative to **2b**.

At first, we performed the geometry optimization for isomers of all the intermediates involved in the catalytic cycle, except for those of the intermediates **2−4**, which we have already published.[23]

Five-Coordinate Complexes. For the starting complex **1**, as shown in Figure 1 two isomers, **1a** and **1b**, are found by MP2/II and RHF/I geometry optimization under the C_s symmetry constraint. Experimentally, the two isomers corresponding to **1a** and **1b** but with PPh$_3$ have been observed in situ by means of NMR spectroscopy,[20] where the latter exists predominantly. The other isomers with an equatorial hydride could be excluded due to the axial preference of hydride, which has been theoretically shown for **3**.[23]

The MP2/II and RHF/I optimized geometries are very similar, except that the metal−CO distance is shorter at the MP2/II level as the electron correlation improves the description of the back-donation effect. The calculated Rh−H bond distance in **1b** is longer than that in **1a** at both RHF/I and MP2/II optimized geometries, which would be ascribed to the strong *trans* influence of a carbonyl ligand compared with a phosphine ligand, as shown previously for (H)$_2$RhCl(CO)(PPh$_3$)$_2$.[29] The CO ligand *trans* to the hydride, which has a stronger σ-donation character than the phosphine ligand, makes the Rh−H bond weaker. The relative stability between **1a** and **1b**, where **1a** is 2.5(MP2/II) or 1.4(RHF/I) kcal/mol lower in energy than **1b**, is inconsistent with the experimental result for PR$_3$ = PPh$_3$ that **1b** is predominant in situ. Although the planar phenyl group causes little steric repulsion,[25b] further studies including the isomerization process between the two structures would be needed to resolve this discrepancy. All equatorial ligands in both **1a** and **1b** are bent toward the hydride ligand by 6−8°, presumably avoiding the steric hindrance.
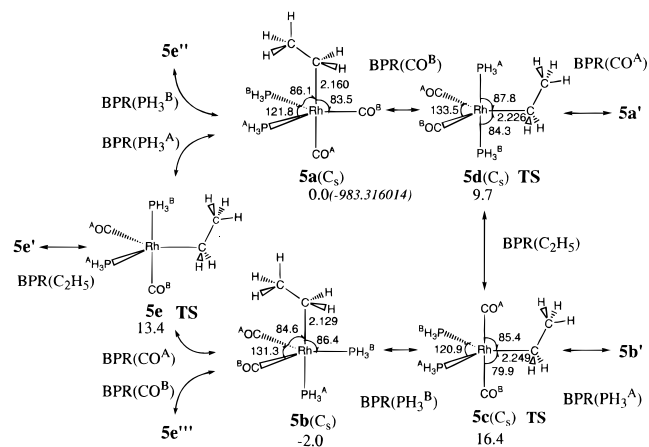
Figure 2. Selected geometrical parameters of optimized structures (Å, deg) for the isomers of intermediate **5** and the potential energy profile (kcal/mol) for isomerization of **5** relative to **5a** (whose total energy in hartrees is given in parentheses) at the RHF/I level.

We just mention that the MP2/II structures in Figure 1 for **3a** and **3b** are similar to RHF/I structures already published,[23] except for the shorter metal−olefin and −CO distances in MP2/II structures, as discussed above. The MP2/II energies of the MP2/II optimized structures are also very similar to those of the RHF/I optimized structures. As seen here and as will be discussed later, the electron correlation changes the relative energies among isomers of the same complex very little and the comparison of different isomers within each complex in this section will be made mainly on the basis of RHF/I energies.

Another five-coordinate intermediate, **5**, has an ethyl ligand in place of the hydride in **1**. There exist five isomers which can be connected mutually through the BPR rearrangement as shown in Figure 2. The geometry optimization was performed under the C_s symmetry constraint. While isomers **5a,b** have stable equilibrium structures, isomers **5c−e** with an equatorial ethyl ligand are not stable, the situation being similar to the axial preference of hydride in **3**. The latter are so unstable that the SPy transition states for BPR disappear and that two successive BPRs to and from them are combined as one.[23] As a result, **5c−e** are the TSs connecting two TBP structures. While **5e** is the TS between **5a** and **5b**, **5d** and **5c** are the TSs connecting **5a** with itself (**5a'**) and **5b** with itself (**5b'**), respectively. Since the rearrangement between two TBP structures could take place through a BPR process, the second-order TSs which have an SPy structure with an apical ethyl ligand would exist between **5c** and **5d** and between **5e** and itself (**5e'**).

There is no large repulsive interaction between the methyl group of the ethyl ligand and two phosphine ligands in the equatorial plane; the energy difference in **5a** between the eclipsed and staggered conformations of the ethyl ligand is about 3 kcal/mol, similar to that for free ethane.[30] The *trans* influence on the Rh−ethyl bond is also observed in Figure 2; the Rh−ethyl bond of **5b** with the phosphine ligand *trans* to ethyl is 0.03 Å shorter than that of **5a** with the carbonyl ligand *trans*

(29) Musaev, D. G.; Morokuma, K. *J. Organomet. Chem.* **1995**, *14*, 3327.

(30) The energy difference between the eclipsed and the staggered conformation for free ethane was calculated to be 2.9 kcal/mol at the RHF/3-21G level.
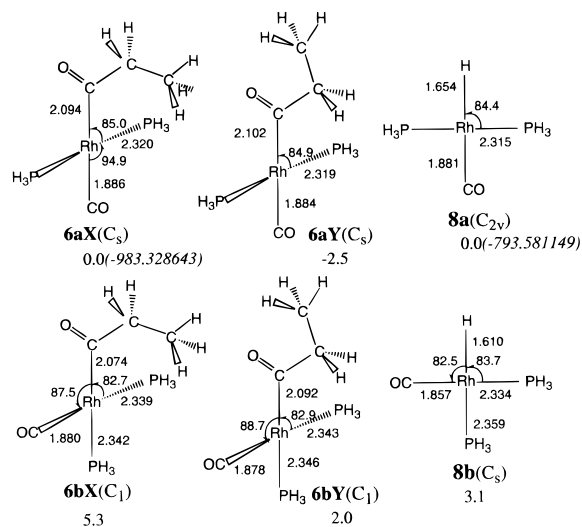
6aX(C_s)
0.0(-983.328643)

6aY(C_s)
-2.5

8a(C_{2v})
0.0(-793.581149)

6bX(C_1)
5.3

6bY(C_1)
2.0

8b(C_s)
3.1

Figure 3. Selected geometrical parameters of optimized structures (Å, deg) for the isomers of intermediate **6** and the energies (kcal/mol) relative to **6aX** (whose total energy in hartree is given in parentheses) at the RHF/I level, as well as for isomers of **8**.

to ethyl. The axial ligands in **5c,d** as well as the equatorial ligands in **5a,b** are bent toward the ethyl ligand to avoid the steric repulsion. The bond angle in the equatorial plane decreases in the order CO−Rh−CO > P−Rh−P > P−Rh−Et > CO−Rh−Et ∼ P−Rh−CO. This tendency, except for the CO−Rh−CO angle, can be understood in terms of steric repulsion between the phosphine ligands. The largest CO−Rh−CO angle would be ascribed to the electronic repulsion between the π electrons of oxygen.

Four-Coordinate Complexes. The four-coordinate intermediates **6** and **8** have *trans* and *cis* isomers, labeled **a** and **b**, respectively. For the acyl complex **6**, we assumed the two stereoisomers labeled **X** and **Y**, which are different from each other in the conformation of the acyl ligand, as presented in Figure 3. In the acyl ligand of isomers **X** and **Y**, the acyl methyl group is *anti* and *syn*, respectively, to the acyl carbonyl group. The geometry optimization was performed under the C_s and C_1 symmetry constraint for the *trans* and *cis* bis-(phosphine) isomers, respectively. **Y**'s are calculated to be more stable than **X**'s. This situation is similar to that of propanal, where it has been known experimentally[31] and theoretically[32] that the most stable conformer has the methyl *syn* to the carbonyl. The energy difference of 2.5 kcal/mol between **6aX** and **6aY** is in good accord with the calculated energy difference of 2.4 kcal/mol between the corresponding conformers of propanal. In **6bX** and **6bY**, the methyl group of the acyl ligand remained *anti* and *syn* to the carbonyl group, respectively, even when the C_s symmetry constraint was released, indicating that they are local minima. The contrast of this result to that for propanal, where minima occur at *syn* and skewed conformations,[30,31] may not be surprising, because the repulsion between the ethyl group of the acyl ligand and the ligands *cis* to the acyl group would be caused by rotation around the C$^{\alpha}$−C$^{\beta}$ bond. The electronically less stable *cis* isomers **6bX** and **6bY**, compared to the corresponding *trans* isomers

(31) (a) Pickett, H. B.; Scroggin, D. G. *J. Chem. Phys.* **1974**, *61*, 3954. (b) Butcher, S. S.; Wilson, E. B. *J. Chem. Phys.* **1964**, *40*, 1671.
(32) Wiberg, K. B.; Martin, E. *J. Am. Chem. Soc.* **1985**, *107*, 5035.

6aX and **6aY**, would become more unstable when the sterically repulsive PPh_3 is used instead of PH_3.

The optimized parameters for the *trans* and *cis* isomers **8a** and **8b** with relative energies are also presented in Figure 3. We assumed C_{2v} symmetry for **8a** and C_s symmetry for **8b.** As one can see in the relative energies, the isomer with *trans* bis(phosphines), **8a**, is more stable than the corresponding *cis* isomer and this energy difference between *trans* and *cis* isomers will increase more in the real system, where PPh_3 is used instead of PH_3, because of the steric hindrance of *cis* bis(phosphines) in **8b**. In contrast, the isomers with *trans* carbonyl ligands, **2a** and **4a**, are less stable than the corresponding *cis* isomers **2b** and **4b**.[23] The Rh−H, Rh−ethyl, and Rh−acyl bonds are influenced by the *trans* ligand; the lengths of these bonds *trans* to phosphine are shorter than those *trans* to carbonyl, again indicating that the *trans* influence of carbonyl is stronger than that of phosphine. All ligands *cis* to a hydride bend toward the hydride to avoid steric repulsion, as in the five-coordinate TBP complexes mentioned in the previous section.

MP2/II optimized structures of **2a,b** given in Figure 1 are similar to RHF/I structures.[23] In the comparison of **1**−**3** in Figure 1, it is concluded that though RHF/I energies cannot be used for comparison of relative energies of three different complexes, the potential energy profile at the MP2/II//RHF/I level agrees well with that obtained by the MP2/II optimization, indicating that the RHF/I structures are acceptable.

Six-Coordinate Complexes. The six-coordinate intermediate **7** is the product of H_2 oxidative addition to the four-coordinate intermediate **6**. Since the H_2 molecule adds to either *cis* or *trans* isomers of **6** in a side-on mode with the H−H bond either parallel or perpendicular to the Rh−acyl bond, as will be discussed later using Scheme 4 , the four *cis*-dihydride isomers are possible, as presented in Figure 4.

Before we investigated the structures of these isomers, three structures of the stereoisomers of **7a** were determined under a C_s symmetry constraint, as also shown in Figure 4, in order to discover which conformation of the acyl group is the most stable. In the acyl ligand, the methyl group can be located *anti*(**7aX**) or *syn*(**7aY,7aZ**) to the acyl carbonyl group, and, in turn, this carbonyl group can be located *anti*(**7aX,7aY**) or *syn*(**7aZ**) to the *cis* hydride ligand. **7aY** is 3.7 kcal/mol more stable than **7aX**, indicating that the *syn* conformation of the acyl ligand is lower in energy than the *anti,* as in **6**, and **7aY** is also 2.8 kcal/mol more stable than **7aZ**.

Therefore, we determined the structures for the other isomers, **7b**−**d** with the acyl ligand having the methyl group *syn* to the acyl carbonyl group and the acyl carbonyl group *anti* to the hydride ligand. C_s symmetry was assumed for **7c** in Figure 4. Although the calculated order of stability is **7a** > **7c** > **7d** > **7b**, the energy differences among the isomers are relatively small; the largest energy difference is only about 2 kcal/mol. As one can notice, however, if we take account of the steric effect of the experimentally used PPh_3, the energies of **7c**, **7d**, and **7b** relative to **7a** would become even higher.
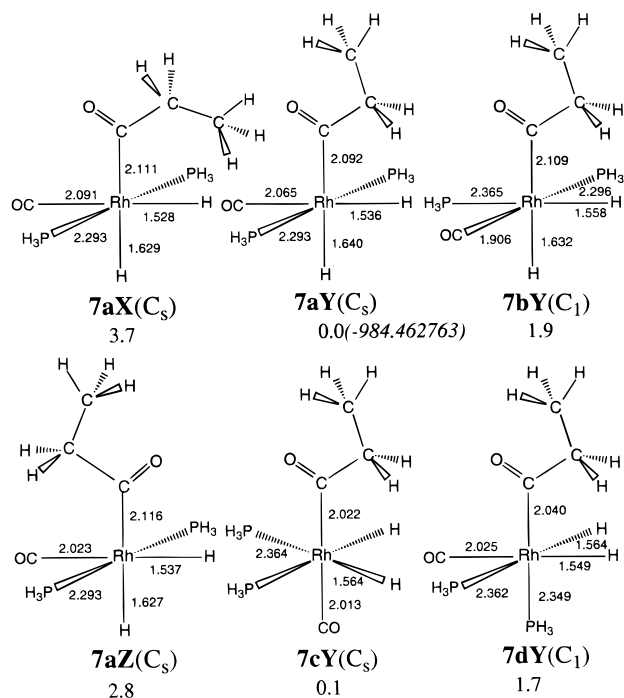
Figure 4. Selected geometrical parameters of optimized structures (Å, deg) of the isomers of intermediate **7** and the energies (kcal/mol) relative to **7aY** (whose total energy in hartrees is given in parentheses) at the RHF/I level.

Elementary Reaction Steps and Their Transition States

The reaction cycle of olefin hydroformylation, as seen in Scheme 1, involves eight elementary reaction steps, four of which pass through transition states: (i) olefin insertion, (ii) CO insertion, (iii) H_2 oxidative addition, and (iv) aldehyde reductive elimination. In this section, at first these four reactions will be examined individually, and at the end the overall potential energy profile will be discussed. We will use Figure 5 as the basis of the presentation. While the comparison in energy of different intermediates and transition states is made at the MP2/II//RHF/I level, the comparison among isomers of a given intermediate or transition state will be based on the RHF/I energies, unless otherwise noted. The RHF/I energy has large unrealistic gaps between **1** and **2** and between **4** and **5**.[33]

Olefin Insertion. We have already investigated the olefin insertion step,[23] and here we only summarize the results. Two isomers, **3a** and **3b**, with axial hydride and equatorial ethylene, are the starting complexes in the ethylene insertion, as shown in Figure 5, where **3a** is 1.7 kcal/mol lower in energy than **3b**. The other much less stable isomers can be excluded from the catalytic cycle. As mentioned in the previous section, *trans* (**4a**) and *cis* (**4b**) isomers exist for the product **4**. The TSs have an SPy structure with basal H and basal ethylene in which the Rh–H bond being broken is parallel to the C=C bond. The skeletal change occurs from the reactant by bending the axial ligands toward the equatorial plane with a little rotation of ethylene, to form the SPy structure in the TS. After the hydrogen migration, the apical ligand moves to the vacant site (former hydride site) to generate **4** with a square-planar (SPl) structure. Consequently, three reaction paths, connecting **3a** and **4b**, **3b** and **4a**, and **3b** and **4b**, are conceivable. In all the cases, the activation barrier is about 20 kcal/mol at the MP2/II or RHF/I level.[23] It has been shown that this activation energy consists of the energy required for deformation of the TBP structure as well as the energy intrinsically needed for bond exchange in olefin insertion.[23] The orbital interactions favoring bond exchange at this SPy transition state will be discussed in the next subsection and compared with the orbital interactions for CO insertion.

CO Insertion. The intramolecular CO insertion takes place in the five-coordinate intermediate **5** to produce the four-coordinate intermediate **6** as shown in Figure 5. We have found that the TSs have TBP-like
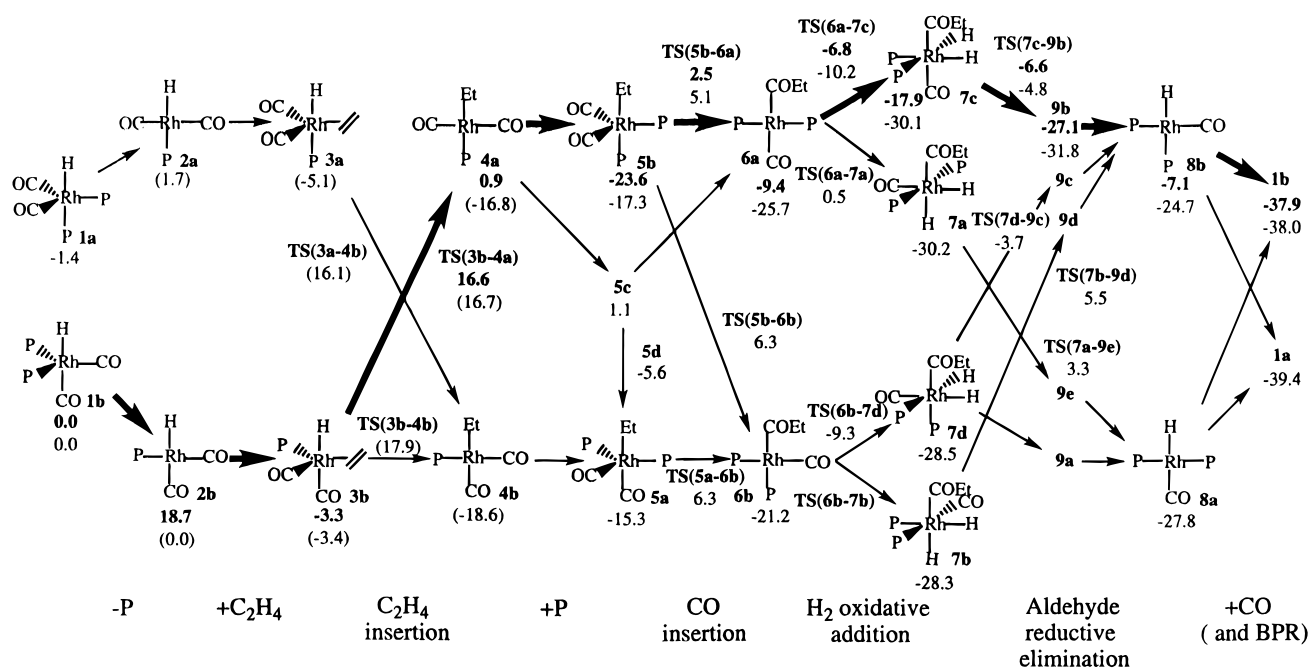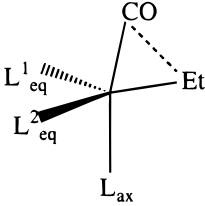

Figure 5. Possible reaction paths for the full hydroformylation catalytic cycle, with the energies (kcal/mol) at the MP2/II//RHF/I (bold) and RHF/I//RHF/I level, relative to **1b** and, in parentheses, relative to **2b**. The energetically most favorable path is indicated by bold arrows.

Table 1. Optimized Bond Lengths (Å) and Angles (deg) of Transition States for the CO Insertion at the RHF/I Level

	L^1_{eq}	L^2_{eq}	L_{ax}	Rh−Et	Rh−CO
TS(5a-6b)	CO	PH_3	PH_3	2.432	1.839
TS(5b-6b)	PH_3	CO	PH_3	2.431	1.841
TS(5b-6a)	PH_3	PH_3	CO	2.406	1.850

	Rh−L^1_{eq}	Rh−L^2_{eq}	Rh−L_{ax}	Et-CO
TS(5a-6b)	1.903	2.375	2.357	2.049
TS(5b-6b)	2.372	1.906	2.356	2.053
TS(5b-6a)	2.344	2.347	1.924	2.090

	L^1_{eq}	L^2_{eq}	L_{ax}	Et−Rh−L^1_{eq}	Et−Rh−L^2_{eq}
TS(5a-6b)	CO	PH_3	PH_3	130.0	103.8
TS(5b-6b)	PH_3	CO	PH_3	102.7	130.6
TS(5b-6a)	PH_3	PH_3	CO	115.5	115.5

	CO−Rh−L_{ax}	CO−Rh−L^1_{eq}	CO−Rh−L^2_{eq}	L^1_{eq}−Rh−L^2_{eq}
TS(5a-6b)	156.8	99.3	92.6	121.3
TS(5b-6b)	156.6	92.8	99.0	121.8
TS(5b-6a)	160.9	94.8	93.9	123.9

Scheme 2. Possible Paths of Intramolecular CO Insertion
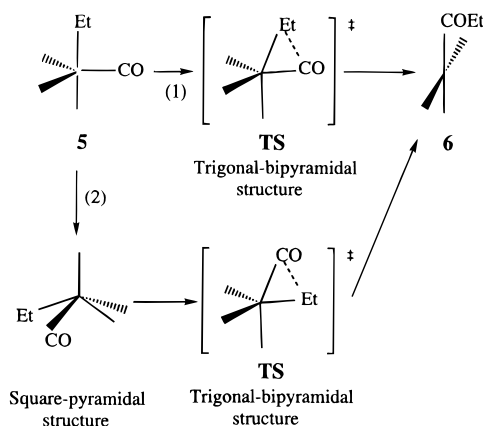
structures with the ethyl in the equatorial plane and the carbonyl at the axial site, in contrast to the SPy structure obtained in the intramolecular ethylene insertion just discussed. Of two possible reaction paths which pass through the TBP transition state shown in Scheme 2, it is path 2 that the reaction chooses. The transition state corresponding to path 1, a path without skeletal change up to the transition state, could not be found and is thus likely to require a large energy because of the deformation of the trigonal-pyramidal structure caused by migration of the ethyl group. On the other hand, path 2 is accompanied by bending of the axial ethyl and carbonyl or phosphine ligands toward the equatorial plane in a manner similar to that in the ethylene insertion step and may pass through

(33) The present use of the subminimal STO-2G basis set for PH_3 in the RHF/I calculation gives unrealistically large PH_3 binding energies, for instance 67.4 kcal/mol for **2b** + PH_3 → **1b** and 68.2 kcal/mol for **4a** + PH_3 → **5b**. When basis set II is used, these become −7.5 and −10.4 kcal/mol, respectively, at the RHF level and 18.7 and 24.5 kcal/mol at the MP2 level.

an SPy-like structure to reach the TBP-like transition state. This skeletal change up to the TS is similar to that in BPR.

We found three TSs with energies similar to each other, as shown in Table 1. The structure of **TS(5b−6a)** is quite close to C_s symmetry except that CH_3 of the ethyl ligand is out of the C_s plane; the Rh−L^1_{eq} and Rh−L^2_{eq} bond lengths and the Et−Rh−L^1_{eq} and Et−Rh−L^2_{eq} bond angles are quite similar. The other two transition states, **TS(5a−6b)** and **TS(5b−6b)**, are enantiomeric with each other except for the conformation of the ethyl ligand. The corresponding bond lengths and angles as well as the relative energies are almost the same among the three TSs. One can notice that the Rh−ethyl bonds are stretched only by 0.2 Å compared with those of the reactants, while the lengths of the newly formed C−C bonds are 0.4 Å longer than those of the products, indicating that the TSs are located early from the viewpoint of bond formation and breaking. The fact that path 2 is more favorable, however, suggests that at the TS the C−C σ bond is partially formed between the CO at the axial site and the attacking ethyl group.
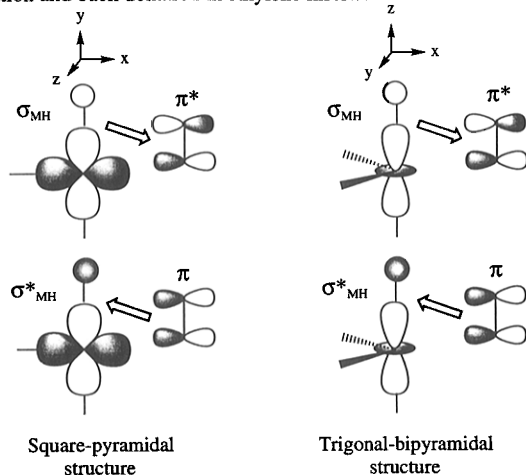
An activation energy of more than 20 kcal/mol at the MP2/II level as well as at the RHF/I level is required for this step. Intramolecular CO insertion in CH_3Pd-(CO)(PH_3)(H) taking place in the C_s symmetry plane was calculated to require an activation energy of 13 kcal/mol at the MP2 level,[3b] suggesting that CO insertion requires an intrinsic activation energy of more than 10 kcal/mol and that the large deformation found in CO insertion into **5** costs about 10 kcal/mol.

The SPy transition state for ethylene insertion of the five-coordinate intermediate mentioned above can be considered to be formed by addition of one extra ligand to the planar TS structure for ethylene insertion of the four-coordinate hydride ethylene complex.[2f] If this thought is extended, the TS for CO insertion into a five-
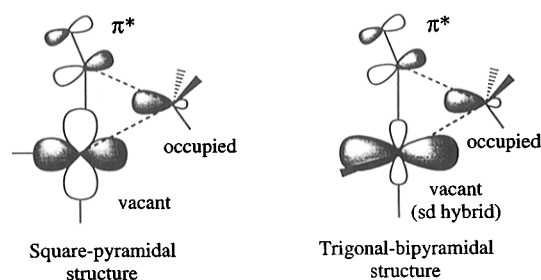
Scheme 3

(a) Donation and back donation in ethylene insertion

Square-pyramidal structure

Trigonal-bipyramidal structure

(b) Three-center interaction in CO insertion.

Square-pyramidal structure

Trigonal-bipyramidal structure

Scheme 4

Square-planar structure

Trigonal-bipyramidal structure

Octahedral structure

TS(6a-7c)(C$_s$) TS(6a-7a)(C$_s$)
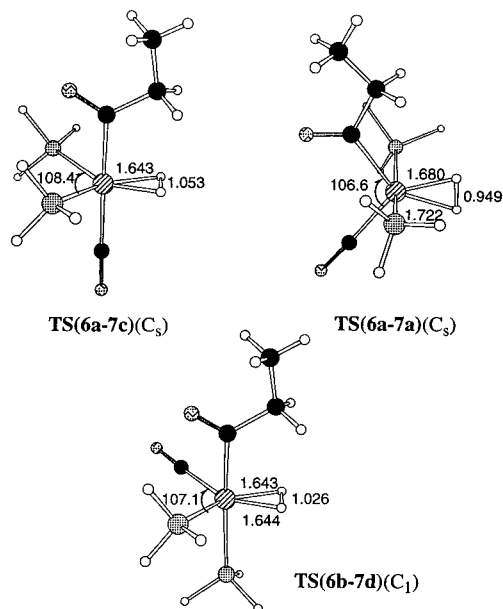
TS(6b-7d)(C$_1$)

Figure 6. Selected geometrical parameters of optimized structures (Å, deg) of the transition states for the H$_2$ oxidative addition at the RHF/I level.

coordinate complex would pass through an SPy transition state because the TS for CO insertion into the four-coordinate methyl carbonyl complex is planar.[3] However, this does not occur. What causes this difference in the structure of the TS between ethylene insertion and CO insertion? As one can see in the BPR rearrangement, the TBP structure is about 3 kcal/mol more stable than the SPy structure.[23] In addition to this energy difference, orbital interactions would control the TS structure for these intramolecular insertions by favoring the structure where stabilizing orbital interactions take place. The orbital interactions in both TBP and SPy structures for ethylene and CO insertions are presented in Scheme 3.[23,34] In the olefin insertion, the Rh—H orbital responsible for the equatorial Rh—C$_2$H$_4$ bonds has contributions from 5s or p rather than 4d orbitals in the TBP structure, though the $4d_{x^2-y^2}$ orbital as well as a 5p orbital mixes into the 5s orbital. Apparently, the σ^*_{MH} and σ_{MH} orbitals, which have contributions from the occupied equatorial d orbitals, $4d_{x^2-y^2}$, in the

SPy transition state, are more appropriate for the four-centered orbital interaction of olefin insertion,[23] both donation and back donation, than those in the assumed TBP transition structure; the orbital interaction overcomes the structural preference. In CO insertion, on the other hand, the structural preference is dominant. As shown in Scheme 3b, the Rh orbital can interact effectively with the migrating ethyl orbital in both SPy and TBP transition state structures, and therefore it is not necessary to deform to the SPy structure costing energy.

H$_2$ Oxidative Addition and Aldehyde Reductive Elimination. There are two possible reaction modes in the H$_2$ oxidative addition step as shown in Scheme 4. The H$_2$ molecule can approach the rhodium atom of **6** with the H—H bond axis perpendicular (path 1) or parallel (path 2) to the Rh—acyl bond. In either path, the reaction would proceed by bending back the two ligands parallel to the H—H bond axis, as is well-known in H$_2$ oxidative addition to SPl complexes.[35]

We first searched the TSs for these two reaction paths in the addition reaction involving **6a**. The optimized structures obtained under the C_s symmetry constraint, **TS(6a−7c)** and **TS(6a−7a)**, are presented in Figure 6. In these TSs, short Rh—H bond distances indicate that the Rh—H bond formation is almost completed; for instance, in **TS(6a−7c)**, the Rh—H bond distances are only 0.1 Å longer than those in the product **7c**. On the other hand, though the H—H bond to be broken is more than 0.3 Å longer than the 0.74 Å bond of the H$_2$ molecule, the H—H bond breaking is not complete, indicating that the bond exchange is asynchronous. The bond angle between the two ligands in the equatorial plane is around 110°, decreasing from 180° in the SPl reactant.

(34) (a) Koga, N.; Morokuma, K. *J. Am. Chem. Soc.* **1985**, *107*, 7230. (b) Koga, N.; Morokuma, K. *J. Am. Chem. Soc.* **1986**, *108*, 6136. (c) Koga, N.; Morokuma, K. *New J. Chem.* **1991**, *15*, 749.
(35) (a) Saillard, J.-Y.; Hoffmann, R. *J. Am. Chem. Soc.* **1984**, *106*, 2006. (b) Ziegler, T.; Tschinke, V.; Fa, L.; Becke, A. D. *J. Am. Chem. Soc.* **1989**, *111*, 9177.
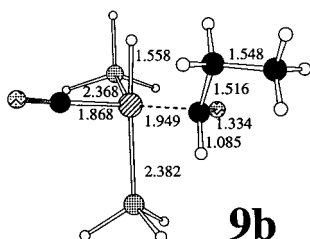
Figure 7. Selected geometrical parameters of optimized structure (Å, deg) of the aldehyde-coordinated intermediate **9b** at the RHF/I level.

By considering the H_2 fragment as a single ligand, one can say that these TSs are five-coordinate and have a TBP structure with H_2 in the equatorial plane. From the viewpoint of electronic structure, the H–H bond is cleaved by simultaneous orbital interactions of electron donation from the H–H σ orbital to the unoccupied sp hybrid σ orbital of the metal and back-donation from the occupied dπ orbital of the metal to the H–H σ^* orbital. The butterfly structure with bent ligands makes those interactions easy, because this deformation of the structure destabilizes the occupied dπ orbitals interacting with the H–H σ^* orbital and stabilizes the sp hybrid accepting electrons from the H–H σ orbital. In this sense, the H–H σ bond at the TSs for H_2 oxidative addition could play a role similar to the ethylene π bond in ethylene coordination. Consequently, the TBP structure of the TSs with the equatorial H_2 plane is favorable.

The energies of these TSs are shown in Figure 5. H_2 oxidative addition to the linear $Pt(PH_3)_2$ complex has been known pass through an early transition state with a low barrier of a few kilocalories per mole because of its large exothermicity.[4a] At the MP2/II level, the present reaction **6a** → **7c** is also exothermic by 9 kcal/mol, and the barrier at **TS(6a–7c)** is only 2 kcal/mol. The acyl ligand which makes a covalent bond with the Rh dσ orbital is expected to prefer the axial position in a TBP structure, similar to hydride and ethyl. The relative energies of the TSs are consistent with this axial preference of the acyl ligand; **TS(6a–7c)** with the axial acyl ligand is about 10 kcal/mol more stable than **TS(6a–7a)** with the equatorial acyl ligand. The difficulty of the latter reaction path may be reflected in the difference in the Rh–H and H–H bond lengths between the two TSs. Apparently, **TS(6a–7a)** is located earlier with the shorter H–H bond and the longer Rh–H bond, though the reaction energies are similar to each other:

In the aldehyde reductive elimination from the isomers of **7**, **7a** with *trans* bis(phosphines) leads to the four-coordinate *trans*-HRh(CO)(PH$_3$)$_2$ (**8a**), **7b** and **7c** with *cis* bis(phosphines) give *cis*-HRh(CO)(PH$_3$)$_2$ (**8b**), and **7d** can give either **8a** or **8b**. Since the acyl carbonyl group is in the vicinity of the rhodium atom in the TS of aldehyde reductive elimination (vide infra), the π bond of its carbonyl group would coordinate prior to aldehyde dissociation to the rhodium atom in the η^2-coordination mode well-known for other complexes.[36] The optimized structure of complex **9b** formed between **8b** and the aldehyde, shown in Figure 7, is similar to
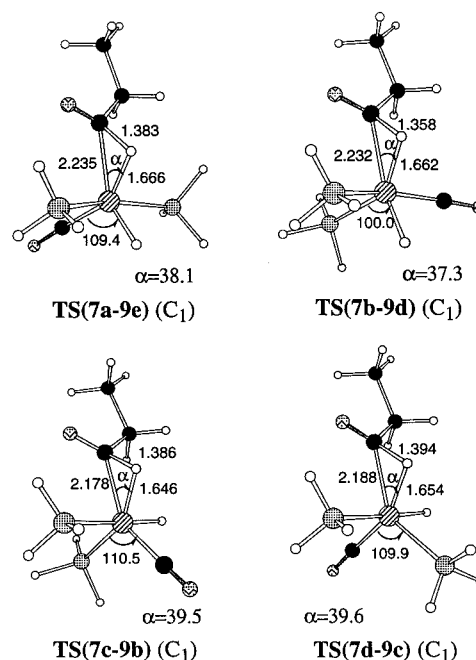
Figure 8. Selected geometrical parameters of optimized structures (Å, deg) of the transition states for the aldehyde reductive elimination at the RHF/I level.

those of ethylene complexes, **3**. The double bond of the aldehyde carbonyl group coordinates horizontally to the rhodium atom in the equatorial plane, and the hydride is at the axial position, as expected from the structural preference observed in **3**. The Rh–carbonyl distance is 0.2 Å shorter than the Rh–ethylene distance in **3**, and the C=O bond is 0.1 Å longer than in a free aldehyde. A similar structure has been determined by X-ray crystallography for $Os(\eta^2$-$CH_2O)(CO)_2(PPh_3)_2$.[37]

The optimized structures of TSs are shown in Figure 8. All the TS structures are TBP, if the partially formed aldehyde is considered as a single ligand. The partially formed C–H σ bond plays the same role as the H–H bond in the TSs for H_2 oxidative addition, and thus the partially formed aldehyde prefers the equatorial plane. Of the remaining ligands, the hydride prefers the axial site, as expected, in the TBP structure. Therefore, **TS(7c–9b)** and **TS(7d–9b)** (and presumably also the uncalculated **TS(7d–9a)**) with axial hydrides are more stable than **TS(7a–9a)** and **TS(7b–9b)** with equatorial hydrides. Since the angle between the two bis(phosphine)–Rh bonds in these transition states is not much decreased from that in the corresponding reactants, the steric effect of bulky phosphines would not change the energy barriers very much. One can notice that, despite the similar energies of reaction, the energetically more favorable **TS(7c–9b)** and **TS(7d–9b)** are earlier than the less favorable **TS(7a–9a)** and **TS(7b–9b)**; the Rh–C and Rh–H bonds to be broken are shorter and the newly forming C–H bond is longer. These structural differences are similar to what was seen in the TS for H_2 oxidative addition.[7]

Potential and Free Energy Profile of the Present Full Catalytic Cycle. By combining the intermediates and the TSs of elementary reactions discussed above,

(36) (a) Tsou, T. T.; Huffman, J. C.; Kochi, J. K. *Inorg. Chem.* **1979**, *18*, 2311. (b) Brunner, H.; Wachter, J.; Bernal, I.; Creswick, M. *Angew. Chem., Int. Ed. Engl.* **1979**, *18*, 861.

(37) (a) Brown, K. L.; Clark, G. R.; Headford, C. E. L.; Marsden K.; Roper, W. R. *J. Am. Chem. Soc.* **1979**, *101*, 503. (b) Clark, G. R.; Headford, C. E. L.; Marsden K.; Roper, W. R. *J. Organomet. Chem.* **1982**, *231*, 335.

Table 2. Calculated Entropy (S), Zero-Point Energy (ZPE) and Potential Energy (ΔE), Enthalpy (ΔH), and Free Energy (ΔG) Relative to 1b in kcal/mol for Selected Intermediates and a Transition State

	ΔE	ZPE	ΔZPE	ΔH^a	S	ΔS	$T\Delta S^a$	ΔG^a
1b	0.0	114.4	0.0	0.0	215.5	0.0	0.0	0.0
2b	18.7	112.0	−2.4	16.4	249.8	34.3	10.2	6.2
3b	−3.3	114.4	0.0	−3.2	213.0	−2.5	−0.7	−2.5
TS(3b−4a)S	15.0	112.9	−1.5	13.7	184.7	−30.8	−9.2	22.9

^{a} $T\Delta S$, ΔH, and $\Delta G = \Delta H - T\Delta S$ calculated at 298.15 K.

one can construct the full catalytic cycle. Since some intermediates and transition states involved in the catalytic cycle have isomers, several catalytic reaction paths can be assembled by connecting them in different ways, as presented in Figure 5. The energetically most favorable reaction path can be extracted by comparing the activation energies among the possible reaction paths, as shown by bold arrows in Figure 5, though often other paths are similar in energy.

First, we look at the catalytic cycle that starts with **1b**, slightly less stable at the MP2/II level (cf. Figure 1) but more stable experimentally than **1a**. **1b** gives **2b**, which leads to **3b**. In the ethylene insertion step, the activation barrier from **3b** to **4a** is the smallest among those of the three possible paths. CO coordination of **4a** leads to **5b**, from which CO insertion takes the path leading to **6a** with a lower barrier than the path to **6b**. The activation barrier for oxidative addition of H$_2$ to **6a** giving **7c** is more than 10 kcal/mol lower than that giving **7a**, and furthermore, the activation energy for aldehyde reductive elimination from **7c** is 9 kcal/mol smaller than that from **7a**. Therefore, the reaction path through **7c** is much more favorable than that through **7a**. Thus the most likely reaction pathway from **1b** is **1b** → **2b** → **3b** → **4a** → **5b** → **6a** → **7c** → **9b** → **8b**. The catalytic cycle starting with **1a** would mainly take the path **1a** → **2a** → **3a** → **4b** → **5a** → **6b** → **7d** → **9a** or **9b** → **8b** or **8a**. The potential energy profile is not very different from that starting with **1b**. Of course, there are many routes connecting these two paths, as seen in Figure 5.

Even if we consider the steric effect of the mutually *cis* bulky PPh$_3$ groups in the real system, the entire behavior of energetics is not expected to change much because it was recently shown that the planar phenyl groups can efficiently avoid steric repulsion of each other.[25b]

The energy difference between the end, **1b** + C$_2$H$_5$-CHO, and the beginning, **1b** + C$_2$H$_4$ + CO + H$_2$, of the entire catalytic cycle is the energy of hydroformylation. At the MP2/II level, the calculated energy of the hydroformylation reaction is −37.9 kcal/mol (exothermic) and the calculated heat of hydroformylation at 298.15 K is −28.5 kcal/mol vs the experimental value of −28 kcal/mol.[38] The large difference of 10 kcal/mol between the energy ΔE and the heat ΔH is due to the zero-point-energy correction, caused by the increase in the number of vibration modes upon conversion of three molecules (C$_2$H$_4$, CO, and H$_2$) to one molecule (C$_2$H$_5$-CHO).

In chemical reactions where the number of independent species changes during the process, the effect of entropy is large and has to be considered explicitly. Obviously, the entropy would favor low coordination

more than high coordination numbers. Therefore, it is expected that the four-coordinate SPl intermediates such as **2b**, **4a**, **6a**, and **8b**, high in the potential energy profile in Figure 5, would be relatively more stable in the free energy profile of the catalytic cycle. We actually calculated the changes in the Gibbs free energy $\Delta G = \Delta H - T\Delta S$ for the step **1b** → **2b** → **3b** as shown in Table 2. On the Gibbs free energy surface the four-coordinate species **2b** is more stabilized by 12.5 kcal/mol relative to the five-coordinate **1b** than it is on the potential energy surface. The free energy of **3b**, relative to **1b**, does not change because they have the same coordination number.

On the basis of the results in Table 2, we have estimated the free energy profile of the entire catalytic cycle by adding to and subtracting from the potential energy an estimated zero-point-energy and entropy contribution of 10 kcal/mol upon each coordination and dissociation, respectively. The reference system, the reactant **1b** with C$_2$H$_4$ + CO + H$_2$, consists of four molecules. The next system, **2b** with PR$_3$ + C$_2$H$_4$ + CO + H$_2$, consists of five molecules, and −10 kcal/mol should be added as a thermal contribution to obtain an estimated free energy. This gives an estimated ΔG of 8.7 kcal/mol, compared to the calculated value of 6.2 kcal/mol in Table 2, with an error of 2.5 kcal/mol. Similarly +10 kcal/mol should be added for all systems consisting of three molecules, **5b**, **TS(5b−6a)**, **6a**, and **8b**, and +20 kcal/mol should be added for two-molecule systems, **TS(6a−7c)**, **7c**, **TS(7c−9b)**, **9b**, and the product **1b** with C$_2$H$_5$CHO. The resultant estimated MP2/II free energies for the catalytic cycle are shown in the fourth column of Table 3. The calculated free energy profile is quite reasonable, without many low-energy traps and high barriers. The highest barrier is at the CO insertion step, and the barrier for the H$_2$ oxidative addition is modest. However, this profile is inconsistent with the experimental observation that the rate is proportional to the pressure of the hydrogen molecule and thus that the H$_2$ oxidative addition step is rate determining.[11c]

Consideration of Solvation Effects

We have so far ignored the solvent effect even though experimentally the reaction takes place in solvent, mostly in hydrocarbons. A justification often used for such an approximation is that hydrocarbon solvent has a low dielectric constant and therefore the solvent effect due to the reaction field should be small. However, hydrocarbon solvent molecules may be able to coordinate strongly to some unsaturated intermediates and transition states and could play an important role in determining the potential and free energy profiles. Therefore, we have investigated the effect of solvent coordination on the energetics of the reaction.

It has been, in fact, a general consensus that the solvent molecule coordinates to, and stabilizes, coordi-

(38) Cornils, B. In *New Syntheses with Carbon Monoxide*; Falbe, J., Ed.; Springer-Verlag: New York, 1980.

Table 3. Potential Energies and Free Energies (kcal/mol) of Important Intermediates and Transition States with and without Solvent Coordination at the MP2/II and MP4SDQ/II Levels at RHF/I Optimized Geometries[a]

	MP2/II				MP4SDQ/II			
	ΔE		ΔG		ΔE		ΔG	
	without solvent	with solvent	without solvent	with solvent	without solvent	with solvent	without solvent	with solvent
1b	0.0		0.0					
2b	18.7	−3.3	8.7	−3.3				
3b	−3.3		−3.3					
TS(3b−4a)	16.6	15.0	16.6	25.0				
4a	0.9	−25.9	0.9	−15.9				
5b	−23.6		−13.6		0.0		0.0	
TS(5b−6a)	2.5	−0.9	12.5	19.1	26.0	22.7	26.0	32.7
6a	−9.4	−33.6	0.6	−13.6	8.8	−8.8	8.8	1.2
TS(6a−7c)	−6.8	−9.5	13.2	20.5	14.0	11.4	24.0	31.4
7c	−17.9		2.1		4.7		14.7	
TS(7c−9b)	−6.6	−9.0	13.4	21.0	17.4	15.1	27.4	35.1
9b	−27.1		−7.1		−0.7		9.3	
8b	−7.1	−33.5	2.9	−13.5				
1b	−37.9		−17.9					

[a] The values with solvent were calculated from the explicit solvent calculation, labeled with **S**, in the text. The values of ΔE are without a zero-point correction, and ΔG is estimated from ΔE with a zero-point-energy and entropy contribution of +10 kcal/mol for each "dissociation" of fragments, as described in detail in the text. MP2 and MP4 energies are relative to **1b** and **5b**, respectively.

natively unsaturated species generated in homogeneous catalytic reactions. For instance, three- and five-coordinate unsaturated intermediates in the catalytic cycle of olefin hydrogenation mediated by the Wilkinson catalyst $RhCl(PPh_3)_3$[39] have been considered to have a solvent molecule at the empty site. Solvation of coordinatively unsaturated species generated by flash photolysis has actually been observed experimentally.[40] In the present case, the reaction experimentally takes place in an alkene solvent. For nonpolar solvents like alkenes, the direct interaction of one or a few solvent molecules is much more important than the long-range interaction via a solvent reaction field.

Solvation of Four-Coordinate Intermediates. Let us consider ethylene as a model alkene solvent. One may note that a solvent molecule of ethylene can coordinate to the four-coordinate intermediate **2b** to give a solvated species **2bS**, which is nothing but the five-coordinate intermediate **3b**. We examined direct coordination of one solvent ethylene molecule to the coordinatively unsaturated intermediates **2b**, **4a**, **6a**, and **8b**. The solvated complexes are denoted by adding **S** to the numbering system, e.g. **2bS**. The geometry optimization was carried out at the RHF/I level, and the energy was calculated at the MP2/II//RHF/I level. The ethylene molecule as solvent was placed roughly perpendicular to the Rh–H, Rh–C_2H_5, or Rh–C(O)C_2H_5 bond axis, on the basis of the site preference of an axial alkyl or acyl ligand as well as that of an axial hydride. C_s symmetry was assumed for **4aS** and **6aS**. The optimized structures of the solvated intermediates **2bS** (≡**3b**), **4aS**, **6aS**, and **8bS** are shown in Figure 9, together with the solvation energies. All four-coordinate intermediates **2b**, **4a**, **6a**, and **8b** were transformed from SPl structures to five-coordinate TBP structures by

ethylene coordination. The two ligands coplanar with the incoming ethylene bend back to form the TBP structure. The Rh–ethylene bond length is about 2.1 Å, the same as that in η^2-ethylene-coordinated complexes. All of the solvated complexes are more than 20 kcal/mol stabilized at the MP2/II level.

Solvation of Transition States. We also examined coordination of one solvent molecule to the TSs between coordinatively unsaturated and saturated species **TS-(3b−4a)**, **TS(5b−6a)**, **TS(6a−7c)**, and **TS(7c−9b)**. For **TS(3b−4a)**, which has an SPy structure, we placed solvent ethylene at the most empty site, *trans* to the apical ligand, and for **TS(5b−6a)**, **TS(6a−7c)**, and **TS-(7c−8b)**, with the TBP structures, we placed it between the two equatorial ligands. C_s symmetry was assumed for **TS(6a−7c)S**. The optimized structures of solvated transition states, **TS(3b−4a)S**, **TS(5b−6a)S**, **TS(6a−7c)S**, and **TS(7c−8b)S**, are shown in Figure 10, together with the solvation energies. In every case, the solvent ethylene was only very weakly bound, with the Rh–ethylene bond distance being ∼5 Å, and caused virtually no skeletal change in the TS structure. The stabilization energy due to the addition of a solvent ethylene molecule is only 1.5−3.5 kcal/mol at the MP2/II level. Because of the long Rh–ethylene distance, no substantial energy difference was found between horizontal (**S1**) and vertical (**S2**) addition of solvent ethylene in the equatorial plane for **TS(6a−7c)**, as seen in Figure 10. These results show that in solution strong coordination to these TBP and SPy transition states would not occur, a situation different from that of the above-mentioned SPl intermediate complexes. This result also suggests that the effect of the second solvent molecule on the structure and energetics of the solvated intermediates **2bS** (≡**3b**), **4aS**, **6aS**, and **8bS** would be small and can be neglected.

When the coordination of solvent is considered, substitution reactions of a solvent molecule with another solvent or ligand molecule may play a role. For instance, a ligand–solvent substitution reaction converting five-coordinate **1b** to a five-coordinate **2bS** may take place by a dissociative mechanism via the four-coordinate intermediate **2b**, or it may take place by an

(39) (a) Osborn, J. A.; Jardin, F. H.; Young, J. F.; Wilkinson, G. *J. Chem. Soc. A* **1966**, 1711. (b) Jardin, F. H.; Osborn, J. A.; Wilkinson, G. *J. Chem. Soc. A* **1967**, 1574. (c) Montelatici, S.; van der Ent, A.; Osborn, J. A.; Wilkinson, G. *J. Chem. Soc. A* **1968**, 1054.

(40) (a) Langford, C. H.; Moralejo, C.; Sharma, D. K. *Inorg. Chim. Acta* **1987**, *126*, L11. (b) Wang, L.; Zhu, X.-M.; Spears, K. G. *J. Am. Chem. Soc.* **1988**, *110*, 8695. (c) Wang, L.; Zhu, X.-M.; Spears, K. G. *J. Phys. Chem.* **1989**, *93*, 2. (d) Simon, D. J.; Xie, X.-L. *J. Phys. Chem.* **1989**, *93*, 291. (e) Lee, M.; Harris, C. B. *J. Am. Chem. Soc.* **1989**, *111*, 8963. (f) Joly, A. G.; Nelson, K. A. *J. Phys. Chem.* **1989**, *93*, 2876.
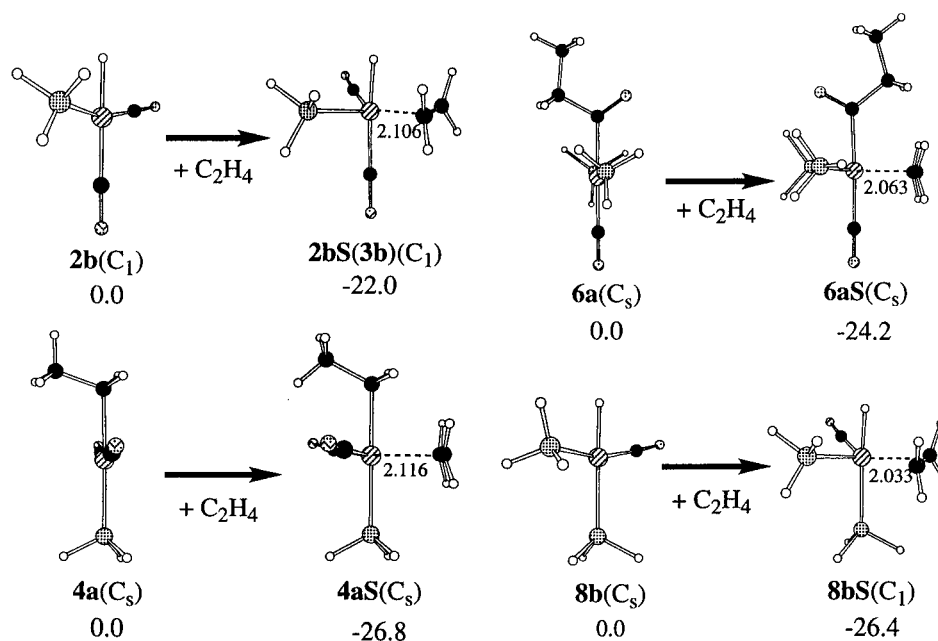
Figure 9. RHF/I optimized structures (Å) for complexes **2bS**, **4aS**, **6aS**, and **8bS** with a solvent ethylene molecule and their energies (kcal/mol) relative to those without solvent ethylene at the MP2/II//RHF/I level.
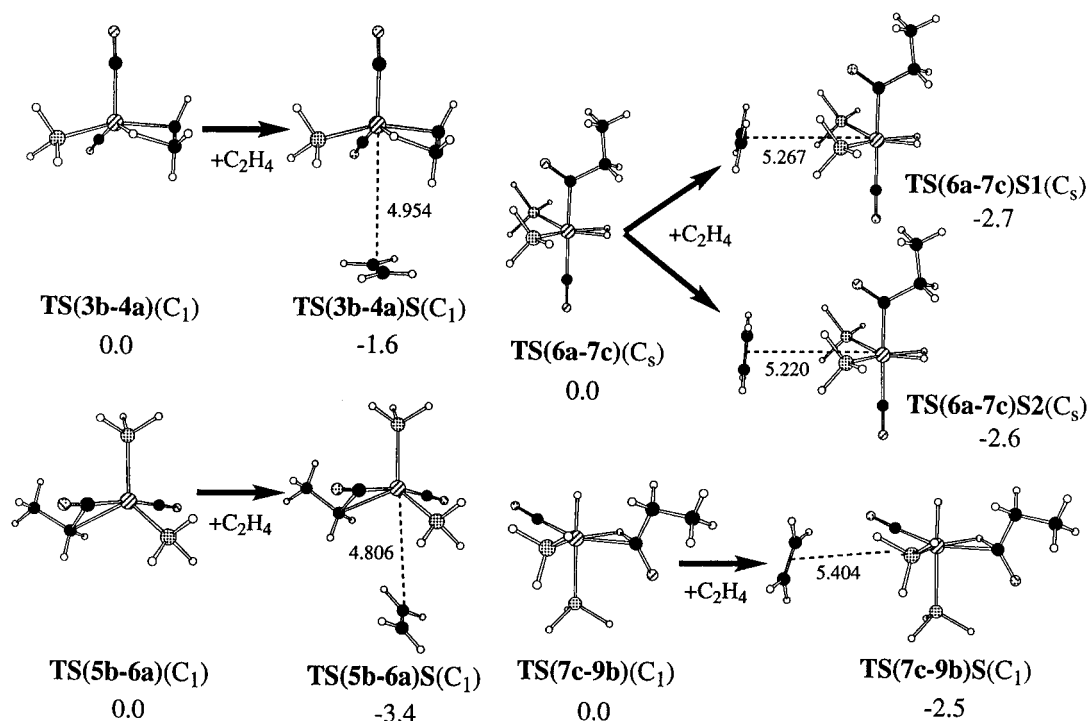

Figure 10. Solvent effect on RHF/I optimized structures (Å) for the transition states in ethylene insertion, **TS(3b−4a)S**, carbonyl insertion, **TS(5b−6a)S**, H_2 oxidative addition, **TS(6a−7c)S**, and aldehyde reductive elimination, **TS(7c−9b)S**, and their energies (kcal/mol) relative to those without solvent ethylene at the MP2/II//RHF/I level.

associative mechanism via a six-coordinate transition state. A similar possibility exists for substitution of a ligand and a solvent between **4aS** and **5b**, **9** and **8bS**, and **8bS** and **1b**. Experimentally, substitution has been found to proceed by a dissociative mechanism for HRh-(CO)(PPh$_3$)$_3$,[41] avoiding unstable 20-electron species.

We performed some model calculations for the substitution of the solvent ethylene in **8aS** by CO. The RHF/I optimized structures and the MP2/II potential energy profile are presented in Figure 11, for both

dissociative and associative mechanisms. The TS for the associative mechanism thus found, with long Rh−C$_2$H$_4$ and Rh−CO distances of about 5 Å, is 3 kcal/mol more stable than **8a** in the dissociative mechanism, indicating that weak interaction remains. Since **8aS** with the TBP structure is expected to be stabilized by weak coordination of CO, similar to coordination of ethylene to **TS(6a−7c)**, the solvation would not greatly affect the barrier height for the substitutions very much; the relatively high barriers remain, indicating the importance of desolvation as well as ligand dissociation in opening the active site.

(41) Kastrup, R. V.; Merola, J. S.; Oswald, A. A. *Adv. Chem. Ser.* **1981**, *196*, 78.
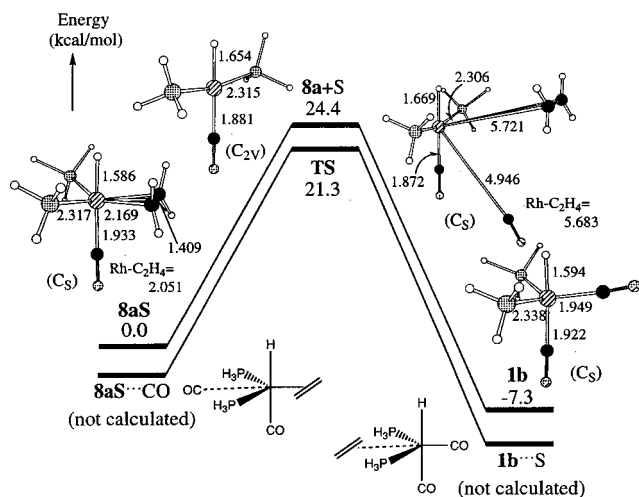
Figure 11. RHF/I optimized structures (Å) and the MP2/II//RHF/I potential energy profile (kcal/mol) for the substitution reaction of **8aS** with CO.

Higher Level Calculations and Final Potential Energy and Free Energy Profiles. In order to obtain the final energetics, we performed higher level, MP3/II and MP4SDQ/II, single-point calculations at the RHF/I optimized geometry, for both solvated and unsolvated species, for the more important second half of the catalytic cycle from **5b** to **9b**. The MP4SDQ/II ΔE values are shown in the sixth and seventh columns in Table 3. The potential energy profile at the MP2/II level is quite similar to that at the MP4SDQ/II level and can be used for semiquantitative discussions, while that at the MP3 level (omitted for brevity) is over 10 kcal/mol away from the others.

Finally, we added the zero-point-energy and entropy contributions to obtain the free energy profile of the catalytic cycle including solvent effects. As in the preceding section, we calculated explicitly the zero-point-energy and entropy contributions for a solvated transition state **TS(3b−4a)S** as shown in Table 2. The entropy contribution causes the solvated transition state **TS(3b−4a)S** to be less stable than the unsolvated transition state **TS(3b−4a)**. This suggests that, in terms of the free energy, coordination of the solvent ethylene to the TSs does not occur, because the extra stabilization energy of only a few kilocalories per mole upon coordination is smaller than the destabilization energy due to the decrease in the entropy. Similarly, the dissociative mechanism should prevail in ligand substitution reactions, since a completely dissociated intermediate such as **8b** is more favorable in ΔG than the TS with a weak interaction. We obtained the free energies for each species, as was done in the preceding section, by adding to and subtracting from the potential energy an estimated thermal contribution of 10 kcal/mol upon each coordination and dissociation, respectively. The reference system, the reactant **1b** with C_2H_4 + CO + H_2 + S (a solvent molecule), consists of five molecules. Entropy contributions of +10 kcal/mol for systems consisting of four molecules, **4aS**, and +20 kcal/mol for three-molecule systems, **6aS** and **8bS**, were assumed. The results are shown as ΔG in Table 3.

Our final free energy profile of the entire catalytic cycle is shown in Figure 12. Here we used ΔG with the MP4SDQ/II method from **5b** to **9b** and ΔG with the MP2/II method for the remainder of the profile. The

connected solid lines are for unsolvated species, and the effects of solvent are shown by arrows (with solvation label **S**). As discussed above, all the transition states are unsolvated. The solvated four-coordinate species, **4aS**, **6aS**, and **8aS**, are the resting stages of the catalytic cycle. For instance, after the CO insertion form **5b** through **TS(5b−6a)**, the intermediate **6a** is stabilized and rests as solvated **6aS**. In the H_2 activation step, **6aS** has to be activated by desolvation to **6a** before it can react with the hydrogen molecule via **TS-(6a−7c)**. The free energy barrier for this step, 23 kcal/mol at the MP4SDQ/II/RHF/I level, consists of the desolvation energy of 8 kcal/mol and the intrinsic activation energy of 15 kcal/mol for the oxidative addition **6 → 7**. In the elementary reaction step where the coordination number increases as in this H_2 oxidative addition, extra energy is required for desolvation. With the solvation effect, this step is very endothermic, while ethylene and CO insertion steps are exothermic and thermoneutral, respectively.

Now, with the desolvation of the intermediate taken into account, the H_2 activation step from **6aS** to **TS-(6a−7c)** has one of the highest barriers in the catalytic cycle. This is consistent with the experimental observation that the rate is proportional to the pressure of the hydrogen molecule and suggests that the H_2 oxidative addition could be one of the rate-determining steps.[13a] Though the CO insertion barrier from **5b** to **TS(5b−6a)** is the highest, CO is involved in various coordination and dissociation stages of the catalysis, as shown in Scheme 1, and its expected pressure dependence is not obvious. For instance, the CO complex of **6**, **13**, has been proposed to be an inactive dead-end trap of the catalytic cycle.[13] Experimentally an increase in the CO pressure has been found to have little effect on, or to even reduce, the overall rate of the catalysis.[13c]

Concluding Remarks

We calculated with the ab initio MO method the potential and free energy profile of the full catalytic cycle of ethylene hydroformylation mediated by the RhH-$(CO)_2(PH_3)_2$ complex. We explicitly considered the effect of the hydrocarbon solvent, which was ignored in past theoretical investigations of reactions of organometallic compounds in solution.

We performed geometry optimization for nearly all isomers of intermediates and transition states involved in each step of the catalytic cycle proposed by Wilkinson et al. The CO insertion step takes place via a trigonal-bipyramidal transition state, in contrast to the olefin insertion step, which proceeds via a square-pyramidal transition state. In the trigonal-bipyramidal transition states for H_2 oxidative addition and aldehyde reductive elimination, as well as in trigonal-bipyramidal equilibrium structures of intermediates, the axial preference of hydride has been demonstrated. Such a site preference at trigonal-bipyramidal intermediates and transition states discriminates among many possible reaction paths and determines the most favorable one.

Solvation of coordinatively unsaturated four-coordinate intermediates by an ethylene molecule as solvent transforms their square-planar structure to a trigonal bipyramid and stabilizes them energetically by more than 20 kcal/mol. By contrast, transition states between coordinatively unsaturated and saturated intermediates
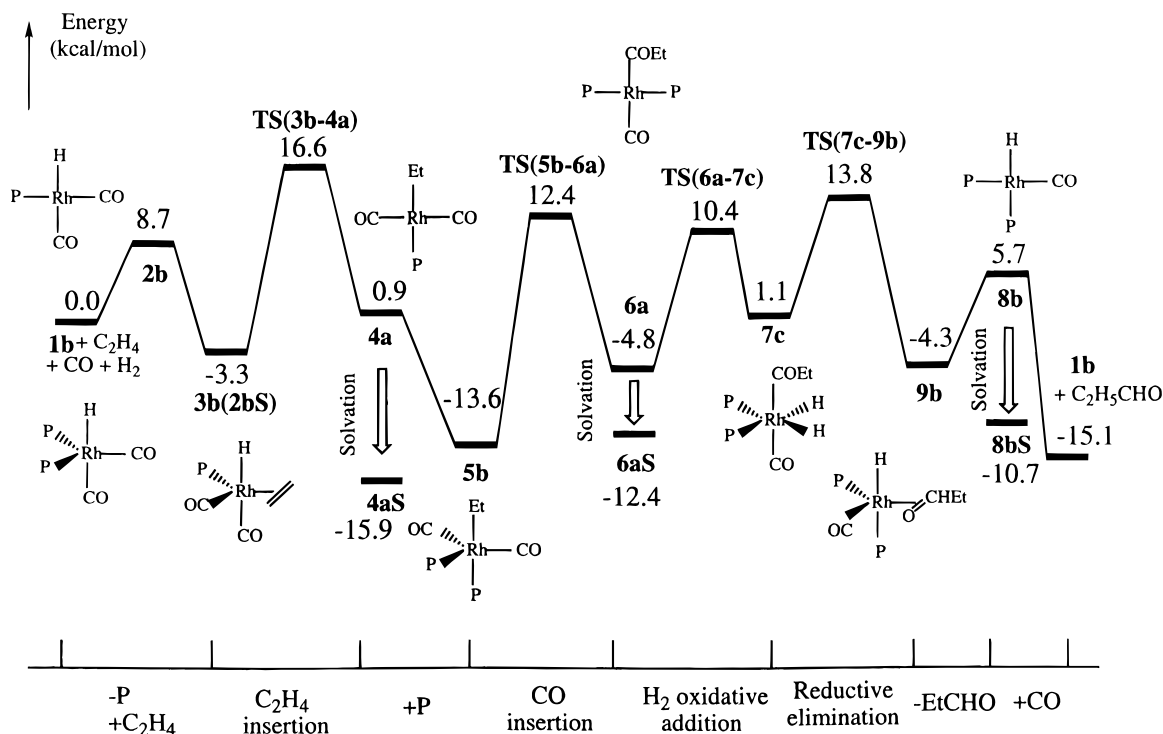
Figure 12. Estimated Gibbs free energy profile (kcal/mol) for the entire catalytic cycle with solvation. The free energy profile without the solvation consideration is given by the solid line, and the effects of solvation are shown by arrows. See text for details.

are stabilized only by a few kilocalories per mole by solvation. The effect of entropy changes upon solvation was also considered. The effect of solvation drastically changes the shape of the free energy profile. The H_2 oxidative addition step in solution has one of the highest barriers in the catalytic cycle and could well be one of the rate-determining steps. In the H_2 oxidative addition, the energy barrier from the solvated intermediate **6aS** is a sum of the desolvation energy of the solvated intermediate and the intrinsic activation energy for oxidative addition to the desolvated coordinatively unsaturated intermediate. We believe this is the first study which has demonstrated that the effect of hydrocarbon solvent plays an essential role in determining the free energy profile of a full catalytic reaction cycle.

As in most theoretical studies in the past, we have used PH_3 as the model phosphine for the experimentally used PPh_3. We recently developed the integrated MO + molecular mechanics (IMOMM) method, in which the active part of the system is handled with an MO method, while the relatively inactive part such as substituents is treated with the MM force field, and applied it to the oxidative addition of H_2 to $Pt(PR_3)_2$ where R = Me, *t*-Bu, and PH.[25] We hope to apply the IMOMM method in the near future to an examination of the steric effect on the present catalytic cycle.